Biomaterials xxx (2014) 1–11

Contents lists available at ScienceDirect

Biomaterials

journal homepage: www.elsevier.com/locate/biomaterials

High-performance PEGylated Mn–Zn ferrite nanocrystals as a passive-targeted agent for magnetically induced cancer theranostics

Jun Xie [a], Yu Zhang [a,*], Caiyun Yan [b], Lina Song [a], Song Wen [c], Fengchao Zang [c], Gong Chen [a], Qi Ding [a], Changzhi Yan [a], Ning Gu [a,**]

[a] State Key Laboratory of Bioelectronics, Jiangsu Key Laboratory for Biomaterials and Devices, School of Biological Science and Medical Engineering, Southeast University, Nanjing 210096, PR China
[b] Department of Pharmaceutics, China Pharmaceutical University, Nanjing 210009, PR China
[c] Jiangsu Key Laboratory of Molecular and Functional Imaging, Medical School, Southeast University, Nanjing 210009, PR China

ARTICLE INFO

Article history:
Received 3 June 2014
Accepted 16 July 2014
Available online xxx

Keywords:
Mn–Zn ferrite nanocrystals
PEGylation
Passive targeting
High-performance
Theranostics

ABSTRACT

An effective magnetic nanocrystals (MNCs)-mediated theranostics strategy as a combination of simultaneous diagnostics and heating treatment of tumors by using magnetic resonance imaging (MRI) and alternating current magnetic field (ACMF) is successfully developed. In this strategy, we had firstly synthesized a well-established Mn–Zn ferrite MNCs coated with PEG-phospholipids (1,2-distearoyl-*sn*-glycero-3-phosphoethanolamine-*N*-[methoxy(polyethylene glycol copolymers, DSPE-PEG2000). The monodisperse PEGylated MNCs with core–shell structure (15 nm) exhibited excellent performance, such as high magnetism of 98 emu g^{-1} Fe, relaxivity coefficient ($r2$) of 338 mM^{-1} s^{-1}, and specific absorption rate (SAR) value of 324 W g^{-1} Fe. It was proved that the obtained MNCs with an average diameter of 48.6 nm can drastically minimize the recognition and phagocytosis of macrophages, simultaneously improve their biocompatibility *in vitro*. These advantages endowed them with efficient passive targeting ability *in vivo* for prominent tumor MRI and magnetically induced heating when exposed to ACMF, based on enhanced permeability and retention (EPR) effects. To ensure sufficient accumulation of MNCs within tumors for targeted hyperthermia, we described the use of MNCs with a well-tolerated intravenous single dose of 18 mg Fe/kg mouse body weight, achieving repeatedly injection and hyperthermia within a subcutaneous breast cell carcinoma mouse model. With an ACMF of 12 A at 390 kHz, the tumor surface sites could be heated to approximately 43 °C in 30 min based on MNCs-mediated intravenous injections. The long-lasting hyperthermia could effectively induce the apoptosis of tumor cells, inhibit the angiogenesis of tumor vessels, and finally suppress the tumor growth within a certain period of time.

1. Introduction

Magnetic nanoparticles (MNPs) have widely received enormous attention in clinical diagnosis and therapy of diseases, because of their unique magnetic properties, facile surface modification, and excellent biocompatibility [1–4]. As a conventional contrast imaging tool, MNPs-based magnetic resonance imaging (MRI) with substantial signal enhancement can help to locate active tumors and determine tumor stages, which has brought significant advances for cancer early detection and diagnosis [1,5,6]. As a promising cancer therapy, MNPs-induced hyperthermia can produce efficient heat induction under an alternating current magnetic field (ACMF), which has been demonstrated in numerous cancerous therapy [4,7,8]. To ensure an optimal strategy for cancer treatment, the MNPs-mediated theranostics by combining simultaneously MRI and hyperthermia, where diagnostics and therapy are integrated into a single platform, has gained increased interest recently [9–12]. In this regard, the theranostics is emerging as an important and beneficial means of triggering various functions of MNPs for personalized clinical application.

The high-performance of MNPs, including superior magnetism, high magnetically induced heating effects, favorable biocompatibility, accurate targeting ability and long circulation, is crucial for their effective theranostics application. High-quality MNPs are typically prepared through a thermal decomposition of organometallic compounds in high-boiling organic solvent containing surfactants, in which some important features, such as shape, size,

* Corresponding author. Tel.: +86 25 8327496 8005.
** Corresponding author. Tel.: +86 25 8327496 8001.
E-mail address: zhangyu@seu.edu.cn (Y. Zhang).

http://dx.doi.org/10.1016/j.biomaterials.2014.07.019
0142-9612/

magnetic dopants, magneto-crystalline phases, and surface states are synthetically controlled [13–16]. Hence, it has proven to be an attractive route for preparing monodisperse MNPs as a promising therapeutic agent with improved crystallinity and superior magnetic properties.

Bare MNPs are rapidly cleared from the blood circulation when passing through the biological defense system and vascular barriers, and mainly accumulate in the liver, spleen, or lymph nodes. Introduction of surface modification, such as amphiphilic molecules, bifunctional polymeric ligands, or biomolecules provides a stabilizing layer that prevents MNPs agglomeration and enhances colloidal stability [1,17–20]. It may help to increase the target-to-background contrast in tumor imaging, and to improve the local concentration of MNPs at the target sites of tumor. The surface modification of MNPs with polyethylene glycol (PEG), known as PEGylation, has become a common method for inhibiting phagocytosis by the reticuloendothelial system (RES), prolonging half-life in blood circulation of MNPs, and promoting the enhanced permeability and retention (EPR) effect *in vivo* [5,6,17–20]. Owing to the EPR effect, intravenously administered PEGylated MNPs extravasate from the vasculature, and preferentially accumulate in tumor tissue, which plays a fundamental role in realizing passive-targeted effects of MNPs. The passive targeting describes the accumulation of MNPs without targeting molecule modification at tumor tissue, but merely exploits the distinct physiology of tumor tissue and the ability of MNPs access to tumor regions by escaping from vascular system. It has the advantages of reducing MNPs uptake in liver and spleen, achieving high concentrations of MNPs in tumor, and limiting the systemic toxicity, which has been predominantly pursued for targeted imaging and magnetic hyperthermia.

Magnetic hyperthermia has recently emerged as a promising therapeutic approach for cancer treatment due to the ability of MNPs to generate heat efficiently when exposed to ACMF. It can directly induce the cytotoxicity of tumor cells above 42 °C for at least 30 min, and cause thermal ablation when heating over 50 °C, leading to the tumor cell necrosis and coagulation under an ACMF with designed fields and frequencies [21,24]. In contrast to the traditional microwave- and radio frequency-induced thermotherapy, magnetic hyperthermia provides a minimal damnification to deliver a therapeutic dose of heat specifically to cancerous regions, which is considered a promising targeting hyperthermia in clinical application [21–24]. It is worthwhile to note that direct intratumoral injection of MNPs followed by induction heating has been widely used in conventional magnetic hyperthermia, which is demonstrated to be safe and beneficial in clinical application [7,25]. They have the advantages of achieving high concentrations of MNPs in tumor regions, and rapidly controlling tumor growth, but severely suffer from tumor incongruence, being invasive, and typically leaving undertreated regions, leading to the cancer regrowth. In contrast, intravenous administration of MNPs covers irregular tumor shapes more precisely, loads many tumors simultaneously and is minimally invasive, which has practical advantages in cancer targeted hyperthermia [7]. An essential challenge in effective targeted hyperthermia based on MNPs-mediated intravenous injections is efficient accumulation of MNPs with high-performance in tumor tissues.

In our study, we develop PEG-phospholipids-coated Mn–Zn ferrite magnetic nanocrystals (MNCs) with specific core–shell structure. It can provide here not only inner cores with excellent magnetism or magnetically induced heating effects, but also external lipid layer with remarkable biocompatibility and biodegradability. More importantly, as both *T*2-weighted MRI contrast agents and hyperthermia agents, the PEGylated MNCs with high-performance are potentially used for tumor passive targeting-based theranostics combinating diagnosis and therapy. The theranostics strategies present here are list as follows: (1) enhancement of MRI contrast in tumors by sufficient accumulation of PEGylated MNCs for accurate detection; (2) evaluation of the therapeutic effect of magnetically-induced hyperthermia with repetitious intravenous injection of MNCs in a safe ACMF with mid-frequency; (3) evaluation of the tumor growth inhibition after the MNCs-mediated effective theranostics.

2. Materials and methods

2.1. Oleic acid (OA)-coated Mn–Zn ferrite MNCs synthesis

The OA-coated Mn–Zn ferrite MNCs were prepared by a thermal decomposition method. In detail, Iron(III) acetylacetonate [$Fe(acac)_3$, 98%, 2 mmol], Zinc(II) acetylacetonate [$Zn(acac)_2$, 96%, 0.4 mmol] and manganese(II) acetylacetonate [$Mn(acac)_2$, 97% 0.6 mmol] were placed in a 50 ml three-neck round-bottom flask in 20 ml benzyl ether (95%), containing 9 mmol OA (90%) and 3 mmol oleyamine (OAm, 90%). They were mixed and stirred under a flow of N_2. The mixture was firstly heated to 220 °C (nucleation temperature) at a heating rate of 3.3 °C/min and refluxed for 1 h. In succession, under N_2 flow with continuous stirring, the mixture was heated to 290 °C (maturation temperature) with a uniform heating rate and maintained at this temperature for 1 h. Lastly, the black-brown mixture was precipitated with external magnet, washed three times using ethanol (95%), and was then dispersed in hexane (99%).

2.2. PEGylated Mn–Zn ferrite MNCs synthesis

A DSPE-PEG2000 (1,2-distearoyl-*sn*-glycero-3-phosphoethanolamine-*N*-[methoxy(polyethylene glycol)], PEG-phospholipids, 99%, Shanghai A.V.T. Pharmaceutical L.T.D. China) was dissolved in 5 ml chloroform. Above-mentioned OA-capped Mn–Zn ferrite MNCs (dispersed in 5 ml hexane) and DSPE-PEG2000 were mixed at 1:2 weight ratio (iron: DSPE-PEG2000) in a 25 ml round-bottom flask, and then, 5 ml deionized (DI) water was added gradually to the mixture. After chloroform and hexane were completely vaporized by slow evaporation (70 °C, 15 min), the MNCs became water soluble. The excess empty lipid micelles were removed from depositing MNCs under a magnetic field, and with repeated ultracentrifugation at 100,000 × *g*. Finally, the obtained MNCs were centrifuged at 3000 × *g* and the large aggregates were discarded. The preparation of PEGylated MNCs was shown schematically in Fig. 1(a).

2.3. 2,3-Dimercaptosuccinic acid (DMSA)-modified Mn–Zn ferrite MNCs synthesis

Ligand exchange with DMSA (Sinopharm Chemical Reagent Co. L.T.D. China) molecules was also carried out to make above OA-coated Mn–Zn ferrite MNCs completely dispersed in aqueous medium [26,27]. In detail, 3 ml OA-capped MNCs (5 mg/ml, dispersed in 12 ml hexane) and 60 mg DMSA (dispersed in 30 ml acetone) were mixed into a 100 ml three-neck flask as well as 150 μl triethylamine were added one after another. After 3 h mechanical stirring and refluxing, black precipitates appeared at the bottom and dissolved in deionized water, demonstrating DMSA had been conjugated onto the surface of MNCs. After further purification by dialysis (MW cutoff of 14 kDa) against deionized water (pH 7) for 2 day, the resultant sample was stored at 4 °C.

2.4. Characterization of PEGylated Mn–Zn ferrite MNCs

The morphology of the as-synthesized PEGylated Mn–Zn ferrite MNCs was observed by using transmission electron microscopy (TEM, Tokyo JEOL, Japan) coupled with high-resolution TEM (HRTEM), in which the samples were dispersed on amorphous carbon-coated copper grids for TEM analysis. The magnetism of MNCs was obtained by a vibrating sample magnetometer (VSM, Lakeshore 7407, USA). The hydrodynamic diameters of MNCs were measured with a particle size analyzer (Malvern Zetasizer, UK). The iron concentrations of MNCs were measured with a classical *C*–*A* (absorbance versus iron concentration) calibration curve, which was established with the 1,10-phenanthroline spectrophotometric method on a UV–visible spectrophotometer (UV-3600, Shimadzu, Japan) [27,28].

2.5. T2-weighted MR imaging in vitro

MRI experiment of PEGylated Mn–Zn ferrite MNCs *in vitro* was carried out on a clinical 1.5 TMR scanner (Avanto, Siemens, Germany). *T*2 relaxation times were determined with a multi-echo spin-echo sequence [16 echoes; repetition time (TR) = 2500 ms; echo time (TE) = 22–352 ms]. For each sample, *T*2-weighted MR images of ten different Fe concentration samples (0.78, 1.25, 1.56, 2.50, 3.12, 5.00, 6.25, 10.00, 12.50, 25.00 μg/ml) were observed. The *T*2 values were obtained by calculating the signal intensity in 0.3 cm^2 region of interest on each image. The relaxivity coefficient (*r*2) as a standardized contrast enhancement indicator was calculated as the gradient of the plot of *R*2 (*R*2 = 1/*T*2) versus the molarity of magnetic atoms [1,13,18].

Please cite this article in press as: Xie J, et al., High-performance PEGylated Mn–Zn ferrite nanocrystals as a passive-targeted agent for magnetically induced cancer theranostics, Biomaterials (2014), http://dx.doi.org/10.1016/j.biomaterials.2014.07.019

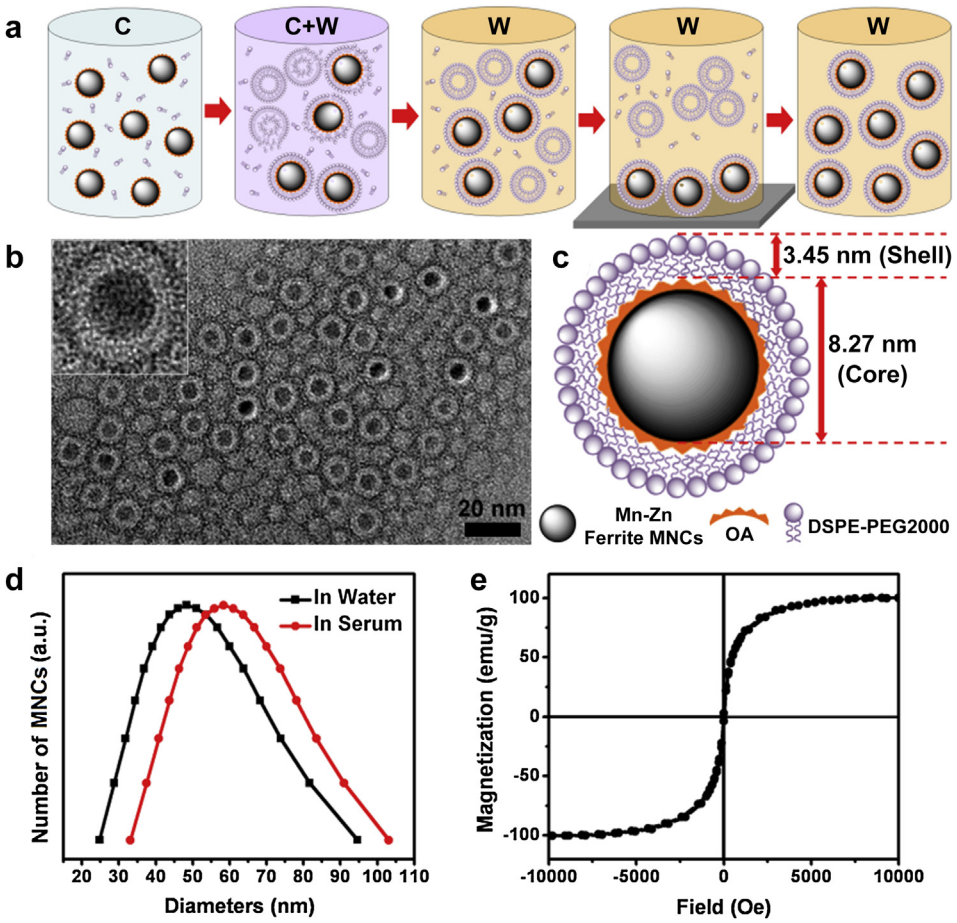

Fig. 1. (a) A schematic diagram of PEGylated Mn–Zn ferrite MNCs synthesis (C: chloroform; W: water). (b) TEM and high-resolution TEM (HRTEM) images of PEGylated MNCs with core–shell structure negatively stained with 2% phosphotungstic acid to give a white layer surrounding the magnetic cores indicating the DSPE-PEG2000 coating layer. (c) A schematic diagram of PEGylated MNCs with 8.27 nm magnetic core and 3.45 nm lipid coating. (d) DLS of PEGylated MNCs in water and serum. (e) Hysteresis loops of PEGylated MNCs.

2.6. Heat induction measurements in vitro

Measurement of heat generation of PEGylated Mn–Zn ferrite MNCs *in vitro* was carried out using a moderate radio frequency heating machine (Shuangping SPG-06-II, China). The samples at uniform concentration (1.2 mg of Fe/ml) were placed inside a copper coil under an ACMF. Specific absorption rate (SAR) is defined as the amount of heat generated per unit gram of magnetic material per unit time, and highly determines the heating ability of MNCs when an ACMF magnetic field is applied (390 kHz, 12 A). The SAR value of MNCs is calculated with the following formula: $SAR = C_w(dT/dt)\,(m_s/m_m)$, where C_w is the specific heat capacity of the suspension (specific heat capacity of water is 4.18 kJ kg^{-1} K^{-1}); dT/dt is the initial slope of temperature versus time graph; m_s is the mass of the suspension, and m_m is the mass of the magnetic material in the suspension [14].

2.7. Cellular uptake and cytotoxicity

RAW 264.7 macrophages were used to measure the unspecific cellular uptake of MNCs. Comparatively, the macrophages were incubated with PEGylated and DMSA-modified Mn–Zn ferrite MNCs of different concentrations (40–160 μg Fe/ml) in each well of a 24-well plate with 10^5 cells per well ($n = 4$ per group). After 12 h, the cells were washed with phosphate buffered saline (PBS) for 3 times, fixed with 4% paraformaldehyde and stained with nuclear fast red for 30 min. To stain the intracellular iron, the Prussian blue solution mixed with of 2% hydrochloric acid aqueous solution and 2% potassium ferrocyanide (II) trihydrate was incubated with the fixed cells for 30 min. After washing with PBS, the cells were placed on a microscope for cellular uptake observation. MTT (3-(4,5-dimethylthiazol-2-*yl*)-2,5-diphenyltetrazolium bromide) assay was used to evaluate the cytotoxicity of MNCs. For MTT assay, the RAW 264.7 macrophages and 4T1 mice breast cancerous cells were incubated in 96-well plates at a density of 10^5 per well and grown overnight ($n = 4$ per group), and then co-incubated with series of concentrations (0, 20, 40, 60, 80, 100 μg Fe/ml) of PEGylated MNCs at 37 °C for 24 and 48 h. Following this incubation, the cells were incubated in media with 0.5 mg/ml of MTT for 4 h. Then the MTT solution was removed and the precipitated violet crystals were dissolved in 150 μl of DMSO. The absorbance was measured at 490 nm with microplate reader. Cell viability was expressed as the percentage of viable cells compared with controls (cells treated with PBS).

2.8. Animal protocol

Female BALB/c mice (4 weeks of age, 20–25 g in weight, $n = 5$ per cohort) were purchased from the Model Animal Research Center of Southeast University. All animal care and experimental procedures were performed according to the Guideline for Animal Experimentation with the approval of the animal care committee of Southeast University. To establish the experimental model of the breast tumor, inoculation with mice breast cancerous cells (4T1, 5×10^6) was accomplished by subcutaneous injection into the legs of mice. The tumors were used for diagnostics and therapy after implantation at 10 days when they were 50–70 mm^3.

2.9. MRI experiments in vivo

In vivo MRI was performed at 7.0 T Micro-MRI (PharmaScan, Brukers, Germany) using a 35-mm birdcage coil and mouse cradle. Mice were initially anesthetized with a 4% isoflurane/air gas mixture delivered through a nose cone and maintained body temperature of 37 °C. MRI of mice was taken prior to the tail vein injection of the PEGylated MNCs and at appropriate time points post injection, which was performed with *T2*, *T2** and diffusion-weighted (DW) flash sequence. The parameters were as follows: *TR*/*TE* = 408 ms/3.5 ms, flip angle = 30°, FOV = 35 mm × 35 mm, slice thickness = 1 mm, matrix = 256 × 256. The total imaging time for each time point was less than 40 min.

2.10. Hyperthermia experiments in vivo

All PEGylated MNCs-induced hyperthermia experiments *in vivo* were carried out safely using a moderate radio frequency heating machine (Shuangping SPG-06-II, 390 kHz, 12 A, China). The mice were placed into the induction coil using a specially

Please cite this article in press as: Xie J, et al., High-performance PEGylated Mn–Zn ferrite nanocrystals as a passive-targeted agent for magnetically induced cancer theranostics, Biomaterials (2014), http://dx.doi.org/10.1016/j.biomaterials.2014.07.019

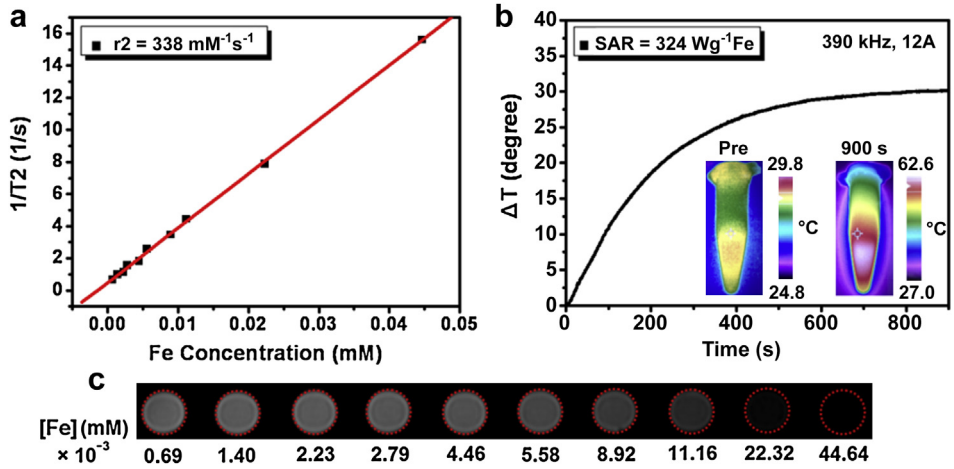

Fig. 2. (a) Dependency of relaxation time of PEGylated Mn–Zn ferrite MNCs upon iron concentration measured by a 1.5 TMR scanner. (b) Time–temperature curves of PEGylated MNCs in aqueous phase (1.2 mg of Fe/ml) under ACMF (390 kHz, 12 A). (c) *T*2-weighted MR images of PEGylated MNCs at various concentrations of iron at 1.5 T.

designed Teflon supporter so that tumors were located exactly in the region of the ACMF possessing the highest field density. Thermal images of mice were taken using an infrared-thermograph (Fulke, Ti32, USA) for temperature measurements. The tumor volumes were calculated from the formula: $V = AB^2\pi/6$, where A is the longer and B is the shorter lateral diameter of the tumor [9]. Relative tumor volumes (ΔV) were calculated as $V - V_0$ (V_0 is the tumor volume when the treatment was initiated).

2.11. Histochemical, biological TEM and immunohistochemistry analysis in vivo

For histochemical analysis, the tumor tissues from mice were excised and fixed in 10% neutral buffered formalin for 1–2 week. Then the tissues were processed routinely into paraffin, sectioned at a thickness of 3–5 μm, stained successively by Prussian blue for ferric ions and nuclear fast red for cell nucleus, or stained by hematoxylin-eosin (HE), and then examined by optical microscopy. The additional sections of tumor tissues were used for terminal deoxynucleotidyl transferase-mediated deoxyuridine triphosphate-biotin nick end-labeling (TUNEL) staining, which was performed with an in situ apoptotic cell detection kit according to the manufacturer's directions (Promega). The apoptotic cells were identified by positive TUNEL staining under optical microscopy, and the four randomly microscopic fields in each group were used to study the percentages of apoptotic cells [29,30].

For biological TEM (JEOL/JEM-2000E, Japan) analysis, tumors tissue after being removed from sacrificed animals were fixed immediately overnight with 2.5% glutaraldehyde, and were further cut into small pieces of ~1 mm^3. In succession, tissue specimens were stained overnight using 1% uranyl acetate in the dark, and were dehydrated using increasing concentrations (from 25% to 100%) of ethanol alcohol. Lastly, the fully dehydrated tissues were embedded in resin, which was then cured in an oven at a temperature of 60 °C (2 days) for TEM observation.

To further examine the heating effects on the microvessels of tumor, an immunohistochemical analysis of tumors was performed. The tumor sections were firstly probed with a monoclonal rat anti-mouse CD31 (vascular endothelial cell marker) antibody (1:400) at 4 °C overnight, following by incubation with biotinylated polyclonal goat anti-rat antibody (1:200), in a humidified chamber for 1 h, and were then immersed in 0.3% H_2O_2 in absolute methanol for 15 min to block endogenous peroxidase. In succession, the sections were counterstained with hematoxylin and mounted with glass coverslips, and were visualized in an optical microscope.

3. Results

3.1. Characterization of PEGylated Mn–Zn ferrite MNCs

The as-synthesized PEGylated Mn–Zn ferrite MNCs consist of a magnetic core of 8.27 nm and a lipid bilayer of 3.45 nm were observed in Fig. 1(b,c). A thin and uniform layer of DSPE-PEG2000 coating was visible in correlative TEM image after negative staining with 2% phosphotungstic acid, showing their homogeneity in size and successful surface modification with no apparent agglomeration. The PEGylated MNCs exhibited a narrow size distribution in water and serum as determined by dynamic light scattering (DLS) (Fig. 1(d)), in which the measured hydrodynamic diameters were 48.6 and 59.2 nm, respectively. Note that the MNCs did not exhibit significant changes in their hydrodynamic diameters even after keeping in aqueous solution and serum for 4 weeks, demonstrating their high colloidal stability [Fig. S1 in the Supporting Information (SI)].

The magnetic characteristic of PEGylated MNCs is crucial for their biomedical applications. As shown in Fig. 1(e), the saturation magnetization (M_s) of PEGylated MNCs was investigated by using VSM at room temperature (300 K), giving an extremely high magnetization value (98 emu g^{-1} Fe). As expected, the hysteresis loop of MNCs showed negligible hysteresis and remarkable superparamagnetism. It was worth mentioning that the high M_s value of the MNCs tended to achieve enhanced MRI contrast effect and distinct magnetically-induced heat generation [10,13]. Specifically, we evaluated the *T*2-weighted MRI contrast effect of above MNCs. As shown in Fig. 2(a,c), the MR signal intensities of the samples were clearly attenuated as the concentration of MNCs increased. The MNCs display a clear concentration-dependent *T*2 signal reduction effect, with a high *r*2 value of 338 mM^{-1} s^{-1}. Moreover, the excellent magnetic heat induction of MNCs in an ACMF could be evaluated by SAR value, as a standard criterion, which was highly dependent on magnetic relaxation and was proportional to the M_s value [1,10,13]. The hydrophilic MNCs (1.2 mg of Fe/ml) induced the temperature elevation by ≈ 30 °C in aqueous solution for 15 min by application of an ACMF (390 kHz, 12 A) and possessed higher SAR values of 324 W g^{-1} Fe [Fig. 2(b)]. The excellent heating effect of PEGylated MNCs meant that they could be potentially applied in cancer hyperthermia *in vivo*.

3.2. In vitro studies of PEGylated Mn–Zn ferrite MNCs

A key consideration for the *in vivo* use of PEGylated Mn–Zn ferrite MNCs is assessing their ability to escape RES uptake and to travel through blood vessels with a reasonably high blood half-life. It is essential to know whether the PEG coating results in a significant decrease of nonspecific uptake of MNCs by RES such as macrophages [5,6]. So we conducted here *in vitro* cell phagocytosis experiments as a prelude to *in vivo* studies, using RAW 264.7 macrophages respectively incubated with PEGylated and DMSA-coated MNCs for comparison. Representative images of macrophages before and after incubation with MNCs for 12 h stained with Prussian blue were shown in Fig. 3(a~g). It could be noticed that most of the macrophages incubated with DMSA-coated MNCs were stained blue, indicating that they tended to be readily

Please cite this article in press as: Xie J, et al., High-performance PEGylated Mn–Zn ferrite nanocrystals as a passive-targeted agent for magnetically induced cancer theranostics, Biomaterials (2014), http://dx.doi.org/10.1016/j.biomaterials.2014.07.019

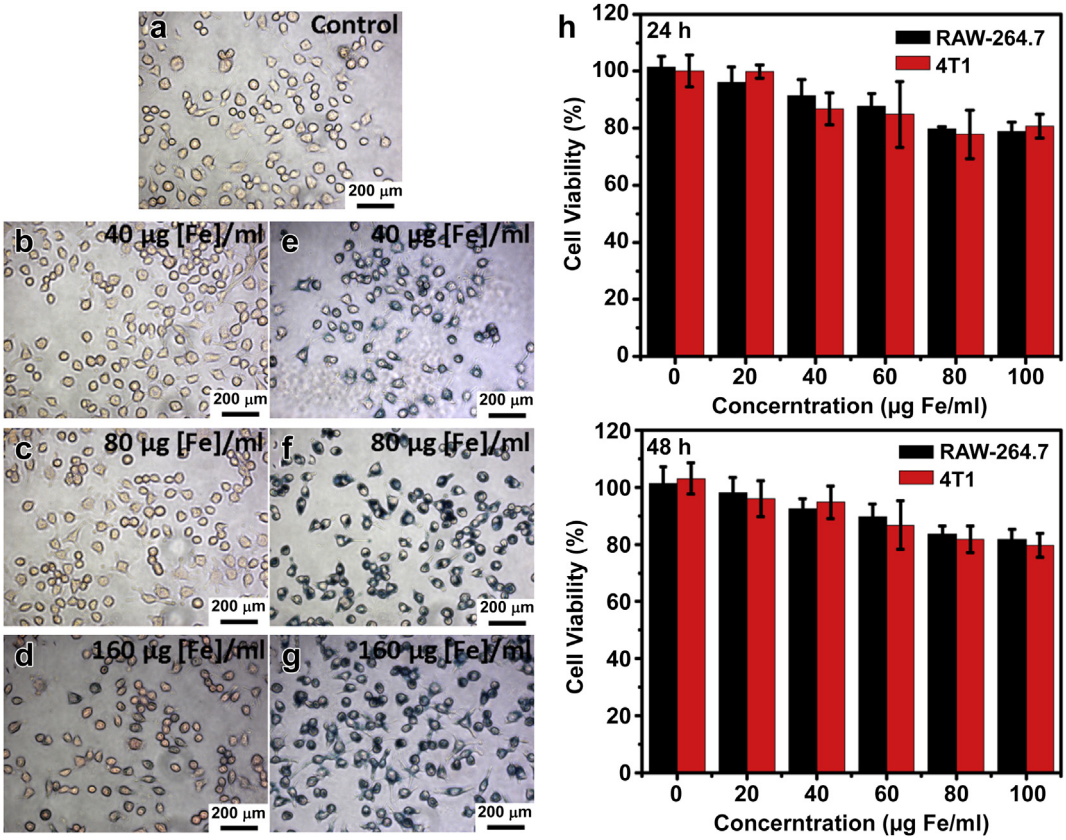

Fig. 3. *In vitro* Prussian blue staining images of macrophages, RAW 264.7, after 12 h treatment with Mn–Zn ferrite MNCs at different concentrations: (a) control, (b–d) PEGylated MNCs, and (e–g) DMSA-coated MNCs. (h) *In vitro* cytotoxicity test of PEGylated MNCs. The viability of the RAW 264.7 and 4T1 cells was determined by MTT assay after incubation with various concentrations of MNCs for 24 and 48 h ($n = 4$).

phagocytosed by macrophages and remained mostly in cytoplasma. Whereas the PEGylated MNCs investigated here led to a no blue color detection as a result of no or significantly lower cell uptake, demonstrating that the PEGylation based on this approach drastically minimized the recognition and phoagocytosis of macrophages.

MTT assay using RAW 264.7 and mouse 4T1 cell lines was performed to analyze the potential toxicity of the PEGylated Mn–Zn ferrite MNCs with various incubation concentrations (20–100 μg of Fe/ml) for 24 and 48 h, as shown in Fig. 3(h). In our past study, PEGylated Fe_3O_4 MNCs showed lower toxicity using RAW 264.7 cells for 24 h, demonstrating their excellent biocompatibility [31]. Comparatively, the PEGylated Mn–Zn ferrite MNCs did not indicate increased cytotoxicity at the same dose. Both of 4T1 and RAW 264.7 cell viability exceed 80% even up to relatively high MNCs concentrations of the 100 μg Fe/ml for 24 or 48 h. The reason might be that the surface lipid modification of MNCs provided a stabilizing layer that prevents the release of toxic ions (e.g. Mn^{2+}), limiting the systemic toxicity.

3.3. *In vivo* MRI of PEGylated Mn–Zn ferrite MNCs and histological analysis

On the basis of the successful *in vitro* experiments, the PEGylated Mn–Zn ferrite MNCs were further used in the subsequent *in vivo* experiments. Generally, the PEGylated MNCs exhibit high resistance to phagocytosis by macrophages *in vitro* as well as low uptake by the liver and spleen *in vivo*, leading to an effective delivery of MNCs to tumor sites through EPR effect [5,6]. To demonstrate the MR imaging ability of tumors, the PEGylated MNCs were injected intravenously into a female BABL/c mouse bearing 4T1 cells with the dose of 9 mg Fe/kg body weight, and $T2^*$-weighted MR imaging in situ was performed using a 7 T MR scanner. The $T2^*$-weighted MR images at the tumor region over time (0–240 min) after the injection were observed in Fig. 4(a). A fraction of the tumor, turned dark as early as 30 min after the injection of the MNCs. With time, this fraction of tumor showing hypointensity became darker and bigger until the duration of 240 min. The distinct MR signal attenuation meant that the PEGylated MNCs passively extravasated from vasculature and preferentially concentrated in tumor region, which could be potentially used as a means of diagnosing the presence of tumors.

To further verify the MRI results and confirm the existence of PEGylated MNCs in tumor tissues, nuclear fast red and Prussian blue stained tumor tissue slices were prepared at 240 min after the injection of MNCs, and analyzed via optical microscopy. As shown in Fig. 4(b) and Fig. S2, the accumulation of the MNCs in tumor tissue could be clearly seen, indicating the existence of many aggregates of stained MNCs. In addition to the tumor tissue slices, other major organs were also stained by similar method. No significant accumulation of MNCs was detected in the heart, kidney and lung, and very small amounts of MNCs were observed in the liver and spleen, indicating the effect of the PEGylation on RES uptake resistance during the blood circulation.

TEM micrographs not only provide the direct evidence of the presence of MNCs in tumor tissues *in vivo*, but also clearly identify where and how MNCs are distributed in tumor cells. The TEM images in Fig. 4(c) provided evidence that PEGylated MNCs were well dispersed in the gaps between the tumor cells (Intercellular substance, IS), or were internalized into the tumor connective

Please cite this article in press as: Xie J, et al., High-performance PEGylated Mn–Zn ferrite nanocrystals as a passive-targeted agent for magnetically induced cancer theranostics, Biomaterials (2014), http://dx.doi.org/10.1016/j.biomaterials.2014.07.019

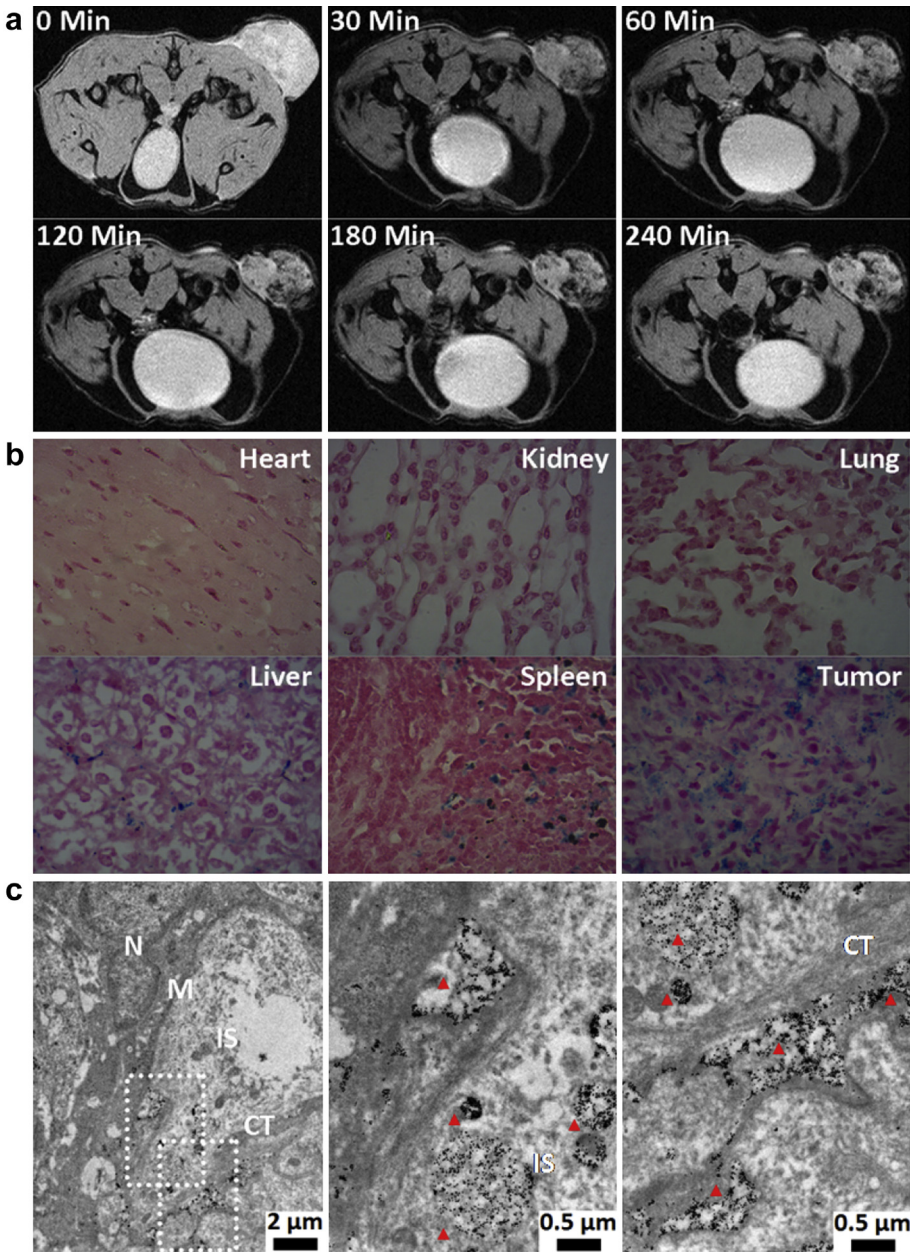

Fig. 4. (a) *T2**-weighted MR images of mice tumor acquired before and after the intravenous injection of PEGylated Mn–Zn ferrite MNCs (9 mg Fe/kg body weight) at different times (0–240 min) using a 7 T MR scanner. After administration of MNCs, the MR signal of the tumor site is significantly attenuated. (b) Nuclear fast red and Prussian blue double staining images (400×) of mouse organs after intravenous administration of MNCs for 240 min (c) TEM image (left) and the corresponding higher magnification (middle and right) of subcellular distribution of MNCs in tumor cells. The red triangle markers indicated the MNCs presented mainly in the IS and CT regions between tumor cells. Remark: N: Nucleus, M: Membrane, IS: Intercellular substance, and CT: Connective tissue. (For interpretation of the references to colour in this figure legend, the reader is referred to the web version of this article.)

tissue (CT) via EPR effect. No significant cellular uptake and intracellular localization of MNCs was observed in tumor tissue. It indicated that the PEGylated MNCs surfaces-mediated tumor passive targeting could reduce efficient binding affinity of MNCS on tumor cell surfaces, leading to the inhibition of uptake and cellular internalization of MNCs.

3.4. PEGylated Mn–Zn ferrite MNCs for cancer theranostics combining MRI and ACMF

Cancer research must overcome the difficulties in tumor detection and orientation, specific tumor treatments, and the control of tumor regrowth. For MNCs, the magnetically induced hyperthermia is a promising cancer therapy, which provides a minimally invasive way to deliver a therapeutic dose of heat specifically to cancerous regions under ACMF. To achieve a tumor treatment prescription, we designed a PEGylated Mn–Zn ferrite MNCs-mediated theranostic system combining MRI and magnetic hyperthermia. The effective tumor-destroying treatment absolutely depends on the high-performance of MNCs and their sufficient accumulation at the tumor sites. In the course of time (usually a few days), PEGylated MNCs may "leak" from the larger pores of fenestrated vascular networks in tumor tissues, leading to the clearance of MNCs by correlative organs (e.g. liver or spleen) *in vivo*. In this

Please cite this article in press as: Xie J, et al., High-performance PEGylated Mn–Zn ferrite nanocrystals as a passive-targeted agent for magnetically induced cancer theranostics, Biomaterials (2014), http://dx.doi.org/10.1016/j.biomaterials.2014.07.019

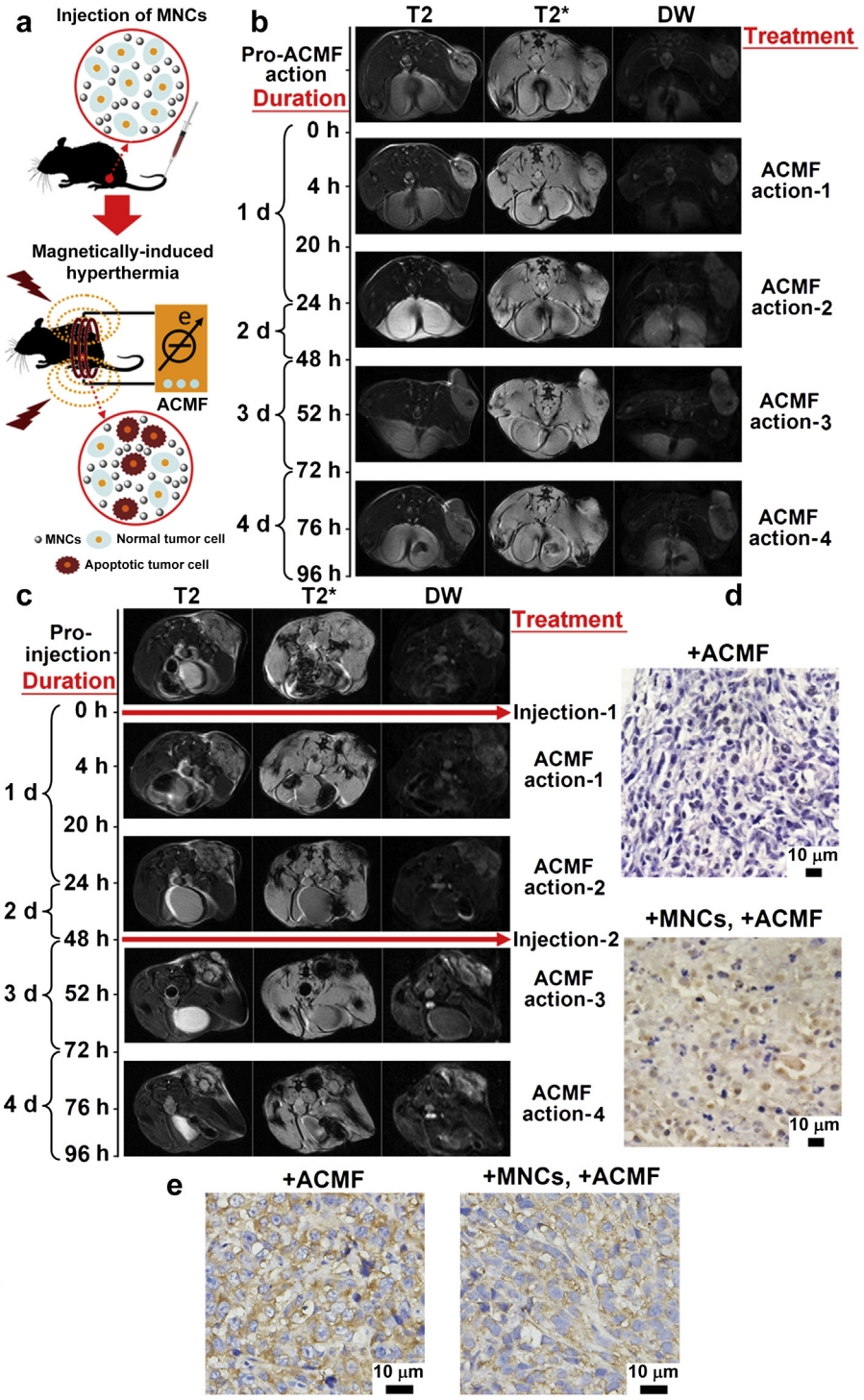

Fig. 5. (a) A schematic diagram of PEGylated Mn–Zn ferrite MNCs as passive-targeted agents for magnetically induced cancer theranostics. (b) *T2*, *T2** and *DW* MR images of mice tumor acquired before and after repeated ACMF actions (390 kHz, 12A) without the intravenous injection of MNCs at different times (0–96 h) using a 7 TMR scanner. (c) *T2*, *T2** and *DW* MR images of mice tumor acquired before and after the repeated intravenous injection of MNCs (single dose: 18 mg Fe/kg body weight) and ACMF actions (390 kHz, 12A) at different times (0–96 h) using a 7 TMR scanner. (d) TUNEL staining assay of mice tumor tissue sections treated and untreated by MNCs under the ACMF actions (390 kHz, 12A). (e) Immunohistochemistry of CD31: the effects of MNCs-induced hyperthermia on the angiogenic profile (brown) of tumor tissue. (For interpretation of the references to colour in this figure legend, the reader is referred to the web version of this article.)

regard, the mice with subcutaneous 4T1 breast cell carcinomas implanted on their legs should be repeatedly treated by higher tail intravenous injection single dose of 18 mg Fe/kg body weight, detected by MRI (*T2*, *T2** and *DW* sequence) in succession, and then were repeatedly heated at least for 30 min (single hyperthermia time) using ACMF of 12 A at 390 kHz [the two injection and four hyperthermia during 96 h (4 days)], as shown in Fig. 5(a). At the diagnostic stages, the *T2**-weighted MR signal intensity at the tumor site decreased significantly after the first injection of MNCs for 4 h, and gradually decreased and reached a maximum after the

Please cite this article in press as: Xie J, et al., High-performance PEGylated Mn–Zn ferrite nanocrystals as a passive-targeted agent for magnetically induced cancer theranostics, Biomaterials (2014), http://dx.doi.org/10.1016/j.biomaterials.2014.07.019

second injection of MNCs for 4 h (cumulative time: 52 h), indicating the effective passive targeting of PEGylated MNCs (*T2** sequence in Fig. 5(c)). Surprisingly, it was observed up to 28 h after the second MNCs injection (cumulative time: 76 h), MNCs-induced MR signal darkening still existed in tumor partial regions. Our results indicated that the long-circulating PEGylated MNCs may effectively and lastingly concentrate in tumor tissues in a certain period. In addition, we simultaneously performed a *DW*-MRI measurement, which provided endogenous image contrast from differences in the motion of water molecules between tissues [32,33], to evaluate the MNCs-induced hyperthermia effectiveness on tumor. The obvious edema was observed surrounding the tumor after the repeated and long-lasting hyperthermia, indicating a positive response to therapy, which was shown by the bright regions in *DW*-MRI [Fig. 5(c)]. No significant changes in morphology and volume of tumors treated by magnetic hyperthermia are observed in *T2*-weighted MR images, meaning the effective inhibition of tumor regrowth. In huge contrast, the tumors of mice without being treated by intravenous injection of PEGylated MNCs but merely placed in an ACMF, gave rise to nearly no obvious signal attenuation but a significant increase in tumor volume based on *T2*, *T2** and *DW* images, which was shown in Fig. 5(b).

TUNEL staining assay was performed here to determine the hyperthermia-induced apoptosis of the cells in the tumor 28 h after the second PEGylated MNCs injection (cumulative time: 76 h) [Fig. 5(d)]. It indicated that the tumors treated with MNCs exposed to ACMF have the extensive regions of apoptotic cells (brown, 63.83 ± 7.08%), and the number of apoptotic cells was significantly more than the one of tumor exposed to ACMF without MNCs injection (apoptotic rate: 5.90 ± 4.79%). Except for the apoptosis of tumor cells, the tumor vascular is also greatly damaged by heating effects. The tumor vasculature develops in a process known as angiogenesis that consists in the formation of new blood vessels from preexisting ones. It is very important for tumor development, which is closely related to tumor regrowth [34–36]. Here the CD31 immunohistochemical analysis of tumors tissue was further to examine the hyperthermia-induced anti-angiogenesis effects. Microvessel density (MVD) is defined as the mean number of microvessels, which is determined by CD31 immunostaining for the new microvasculature of the tumor tissue [34,35]. On the immunohistochemical images [Fig. 5(e)], the tumors showed a heterogeneous vascularization with large, intensively branched vascular networks (brown stained). The calculated MVD (numbers per 400 × field) was significantly decreased in the MNCs-treated group of tumor exposed to ACMF, relative to the tumor group acted only by ACMF without MNCs injection (65.76 ± 7.34 *vs* 43.61 ± 4.17, $P < 0.05$), showing a remarkable vascular damage. We therefore concluded that MNCs-induced hyperthermia resulted in increasing the apoptosis of cancer cells, and inhibiting the angiogenesis of tumor tissue.

The sufficient temperature elevation and heating duration play crucial roles for PEGylated MNCs-induced targeted hyperthermia, which is based on the increased MNCs injection dose and multiple hyperthermia periodicities. Continuous temperature up to 42 °C can render cancer cells more susceptible to the heating effects and cause a certain degree of apoptosis. We described a MNCs-mediated tumor theranostics strategy for more reduplicative and long-lasting MNCs injection (4 times) and hyperthermia (8 times) in 12 days, to achieve a more effective therapy (Table 1). In the past, a fiber-optic thermocouple was placed in the tumor interior in test animals to measure temperature change in tumors, at the expense of causing leakage of the gelatinous tumor parenchyma [7,8]. Herein, the thermal images (measured with an infrared camera) of a mouse after repeated MNCs injection (3–4 times) and hyperthermia (5–8 times) under an ACMF were used to directly detect

Table 1
The strategy of PEGylated Mn–Zn ferrite MNCs as passive-targeted agents for magnetically induced hyperthermia.

Days	MNCs intravenous injection (times)[a]	MNCs-based hyperthermia (times)[b]
1	1	1
2	–	2
3	2	3
4	–	4
5	3	5
6	–	6
7	4	7
8	–	8
9	–	–
10	–	–
11	–	–
12	–	–

[a] Repetitious Intravenous injection of MNCs at single dose of 18 mg Fe/kg body weight every other day.
[b] Sufficient hyperthermia duration (30 min) every day (with an ACMF of 12 A at 390 kHz).

the tumor surface temperature [Fig. 6(a)]. The difference of tumor interior and surface is almost ±2 °C, so the external temperature of tumor is used to potentially evaluate the hyperthermia effects so as not to invasively disturb tissues [7]. As shown in Table 2, the surface temperature of tumor was higher than the surrounding tissues by ≈ 6–10 °C after repeated hyperthermia treatment, and the local maximum temperature achieved is 43.8 °C, which was capable of inducing the apoptosis of tumor cells, and inhibiting the angiogenesis of tumor simultaneously. During eight ACMF exposures, tumor volumes were measured and recorded in 12 days [Fig. 6(b,c)]. The tumor growth rates were markedly attenuated in the mice placed in an ACMF after injection of MNCs. By comparison, a significant increase in tumor volumes with only ACMF exposure (no MNCs injection) was observed in tumor photographs and growth curves. These results indicated that the MNCs-mediated hyperthermia ultimately resulted in delay in the tumor growth within a certain period of time.

In addition, it might be noted that we had found no significant apoptosis and vascular damage of tumor tissue after MNCs administration but without ACMF exposure, as indicated by histochemical and immunohistochemistry analysis *in vivo* (Fig. S4), in despite of widespread distribution of MNCs in tumor region (Fig. S3). Accordingly, we had also observed a trend toward increased tumor volumes in only MNCs group (no ACMF) in 12 days (Fig. S5). This was consistent with our *in vitro* work, which had indicated that the MNCs had a lower cytotoxic effect on breast cancer 4T1 cells, based on the biocompatibility of MNCs external lipid bilayer. The effect of MNCs administration alone therefore would not remarkably induce the tumor cell death and inhibit the tumor growth.

4. Discussion

Herein, the EPR effect is considered to be a landmark principle in our PEGylated Mn–Zn ferrite MNCs-induced tumor passive targeting by intravenous administration. After the adequate passive accumulation of MNCs at the tumor sites via the EPR effect, MNCs-mediated tumor therapeutics has the potential to simultaneously image and hyperthermia using by MRI and ACMF, where therapy and diagnostics are integrated into a single nanocrystals platform. To greatly improve the cancer therapeutic efficacy based on the MNCs passively accumulated into tumor tissue, several key factors in MNCs synthesis are established as follows.

Firstly, it is well known that the magnetic characteristic of MNCs is crucial for their successful theranostics performances. Generally,

Please cite this article in press as: Xie J, et al., High-performance PEGylated Mn–Zn ferrite nanocrystals as a passive-targeted agent for magnetically induced cancer theranostics, Biomaterials (2014), http://dx.doi.org/10.1016/j.biomaterials.2014.07.019

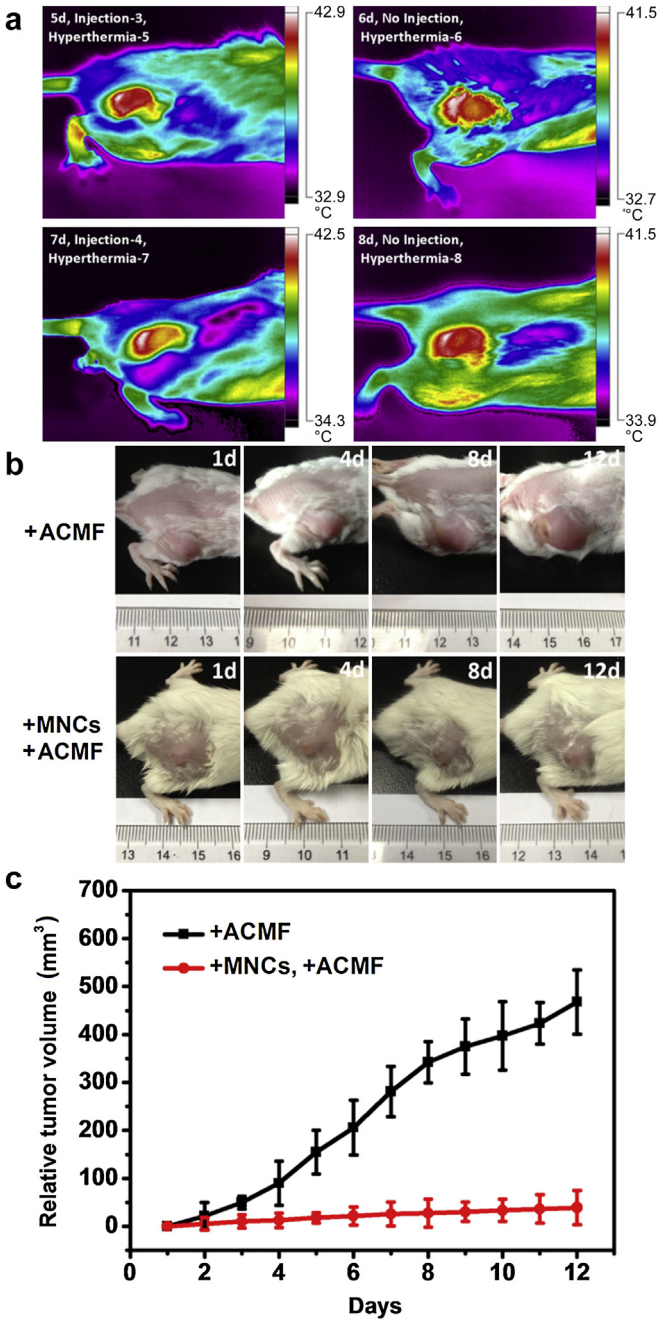

Fig. 6. (a) Thermal images of a mouse after intravenous injection (3–4 times) and magnetically-induced hyperthermia (5–8 times) using PEGylated Mn–Zn ferrite MNCs under an ACMF with 390 kHz and 12 A. (b) Photographs and (c) tumor growth behavior of mice without treatment and treated by intravenous injection of MNCs under the repeated ACMF actions (390 kHz, 12 A) in 12 days.

the magnetism of nanoparticles can be greatly influenced by doping with magnetically susceptible elements. The metal–doped MFe_2O_4 nanoparticles in which Fe^{2+} ions are replaced by other transition–metal dopants M^{2+} (M=Mn, Zn, Ni, Co) have been pursued to achieve larger magnetocrystalline anisotropy and higher magnetic susceptibility, compared with conventional Fe_3O_4 and γ-Fe_2O_3 MNPs [1,4,13]. In this regard, our synthesized doping Mn–Zn ferrite MNCs are proved to exhibit extremely high magnetization value (98 emu g^{-1} Fe). The outstanding magnetic-performances make the MNCs promising as an excellent material for early diagnosis and therapy *in vivo*.

Secondly, the size distribution and surface modification of MNCs are also vitally important for facilitating their biodistribution and circulation *in vivo*. The apparent size of MNCs is highly related to their capabilities for effectively overcoming the biological defense system and vascular barriers. In detail, very smaller particles (<10 nm) may leak from first-pass elimination by the kidney, while larger particles (100 nm to several μm in size) are easily cleared by the mononuclear phagocyte system (MPS) and occur primarily in the liver and spleen [1,37–40]. Hence the nanoparticles with sizes of 10–100 nm are ideal for their long retention time in blood circulation *in vivo*. In the designs of MNCs with surface modification, PEGylation is also an effective method for prolonging blood circulation, reducing MPS uptake and promoting superior EPR accumulation in tumor tissues. Herein, an emerging design in surface modification is the incorporation of a hydrophilic phospholipid-PEG (DSPE-PEG2000) on the surface of individual MNCs via hydrophobic interaction (Fig. 1(b,c)). The monodisperse core–shell PEGylated MNCs with narrow size distribution in water indicate excellent MRI contrast effects and magnetocaloric effects ($r2$ relaxivity of 338 $m_M^{-1}s^{-1}$ and *SAR* value of 324 W g^{-1} Fe). In virtue of the external PEGylated lipid layer with favorable biocompatibility, the MNCs exhibit no obvious cytotoxicity *in vitro* [Fig. 3(h)], and are observed to have a reduced liver and spleen uptake, but a significant increase in tumor uptake *in vivo* (Fig. 4). These advantages of PEGylated MNCs endow them high efficiency in tumor MR imaging through established passive targeting strategies at a relatively low dose.

The extraordinary strategies of PEGylated MNCs-mediated tumor theranostics attained in our study can be attributed to a combination of five factors: (1) use of a ACMF with moderate frequency and field for effective heating effects, (2) size of ACMF helical coil device, (3) adequate intravenously injection dose and passive accumulation of MNCs into tumor, (4) repetitious MNCs-administered injections every other day, (5) sufficient hyperthermia duration every day. Although small amounts of MNCs accumulated in the liver and spleen, our designed ACMF system focused the heat into very small tumor regions and promoted higher thermal energy production. The optimization of ACMF with adequate frequency and helical coil device provides the base for theranostics strategies. Herein the tumor region of a mouse is placed in the center of magnetic induction coil device with appropriate size (3 cm in diameter and 1.5 cm in length) in ACMF, which is used for making magnetic hyperthermia a more effective approach to cancer therapy with a decreased risk of heating surrounding healthy tissues (e.g. liver and spleen). No obvious pathological changes are observed in corresponding HE stained histopathology images of mice liver and spleen tissue sections (Fig. S6). For clinical application, there is also concern about eddy current heating in normal tissues at high fields and frequencies (above 500 KHz), which are harmful for the health of the patients. In contrast to conventional low-frequency ACMF (10–100 kHz) for clinical tumor hyperthermia, our designed mid-frequency ACMF of 12 A at 390 kHz has been demonstrated safety and beneficial for potential application [41,42], which is suggested to be more useful for efficient heat induction in the region of tumor tissue containing MNCs (heat centers).

To obtain long-lasting and effectively hyperthermia in tumor, the dosages of MNCs (four injection, single dose of 18 mg Fe/kg body weight) used here is considerably larger than that used in previous MR imaging. At this level in mice, it is observed no obvious clinical signs of toxicity (no weight loss or abnormal behavior) over the course of 4 weeks. The repeated intravenously injections of MNCs produce adequate MNCs coverage in tumor intercellular substance and connective tissue [Figs 4(c) and 5(c)], and are powerful enough to effectively heat up to approximately 43 °C in corresponding tumor surface sites when exposed to ACMF for 30 min [Fig. 6(a)]. Furthermore, the repeated hyperthermia-

Please cite this article in press as: Xie J, et al., High-performance PEGylated Mn–Zn ferrite nanocrystals as a passive-targeted agent for magnetically induced cancer theranostics, Biomaterials (2014), http://dx.doi.org/10.1016/j.biomaterials.2014.07.019

Table 2
Temperature indication of tumor surface after the PEGylated Mn–Zn ferrite MNCs-induced hyperthermia detected by thermal images.[a]

MNCs-based hyperthermia (times)	Average temperature (°C)	Maximum temperature (°C)	Minimum temperature (°C)
1	40.2	41.3	37.7
2	39.4	40.6	38.9
3	41.5	42.3	39.2
4	41.2	41.9	38.8
5	42.9	43.8	40.6
6	41.3	42.6	39.6
7	42.1	43.6	40.1
8	41.2	42.0	39.6

[a] Parallel group $n = 5$.

induced temperature elevations in tumor tissues initiate a series of subcellular events, rendering the raise metabolism and transition of targeted cellular structures, and the cells susceptible to various forms of damage including apoptosis and cytoclasis [Fig. 5(d)]. Subsequently, the durable heating effects are shown to alter the tumor microenvironment in terms of hypoxia, perfusion in tumors and immunological function, leading to tumor tissue necrosis and coagulation, which effectively inhibit the tumor growth within a certain period of time [Fig. 6(b,c)].

5. Conclusions

In summary, we have successfully developed a monodisperse lipid-PEGylated Mn–Zn ferrite MNCs with ideal core–shell structure and excellent performance. The advantage of the PEGylated MNCs here depends on not only the inner magnetic cores with high-quality magnetism and magnetic heating effects, but also the external PEGylation shells which greatly prolong blood circulation, reducing MPS uptake and improve the biocompatibility *in vitro*. The intravenous administrated MNCs are proved to effectively passive-targeted accumulate in tumor tissues via the EPR effect, which plays a fundamental role in their successful cancer targeted magnetic hyperthermia performances. To greatly increase magnetically induced heat generation for tumor, our strategy is increasing intravenously injection dose of MNCs and MNCs injection times, and actualizing repeatedly sufficient hyperthermia duration under an designed ACMF (390 kHz, 12A), accompanied by a real-time detection and diagnosis of tumor using by MRI. It is emphasized that the long-lasting MNCs-mediated heat induction in tumor effectively inhibits the tumor growth within a certain period of time. The current developmental stage of theranostic MNPs is still too early to predict their success, but we believe our synthesized PEGylated MNCs with outstanding magnetic-performances as excellent MRI and heating agents, further combined with targeted molecules and anticancer drugs, have more promising cancer theranostics applications.

Acknowledgment

This research was supported by the National Basic Research Program of China (No. 2011CB933503, 2013CB733800), National Natural Science Foundation of China (No. 31170959), National Key Technology Research and Development Program of China (No. 2012BAI23B02), the Basic Research Program of Jiangsu Province (Natural Science Foundation, No. BK2011036) and Jiangsu Provincial Special Program of Medical Science (No. BL2013029).

Appendix ASupplementary data

Supplementary data related to this article can be found at http://dx.doi.org/10.1016/j.biomaterials.2014.07.019.

References

[1] Jun YW, Lee JH, Cheon J. Chemical design of nanoparticle probes for high-performance magnetic resonance imaging. Angew Chem Int Ed 2008;47:5122–35.
[2] Yu MK, Jeong YY, Park J, Park S, Kim JW, Min JJ, et al. Drug-loaded superparamagnetic iron oxide nanoparticles for combined cancer imaging and therapy in vivo. Angew Chem Int Ed 2008;47:5362–5.
[3] Chen ZW, Yin JJ, Zhou YT, Zhang Y, Song LN, Song MJ, et al. Dual enzyme-like activities of iron oxide nanoparticles and their implication for diminishing cytotoxicity. ASC Nano 2012;6:4001–12.
[4] Lee JH, Jang JT, Choi JS, Moon SH, Noh SH, Noh SH, et al. Exchange-coupled magnetic nanoparticles for efficient heat induction. Nat Nanotechnol 2011;6:418–22.
[5] Liu DF, Wu W, Ling JJ, Wen S, Gu N, Zhang XZ. Effective PEGylation of iron oxide nanoparticles for high performance in vivo cancer imaging. Adv Funct Mater 2011;21:1498–504.
[6] Lee N, Choi Y, Lee YJ, Park M, Moon WK, Chio SH. Water-dispersible ferrimagnetic iron oxide nanocubes with extremely high r2 relaxivity for highly sensitive in vivo MRI of tumors. Nano Lett 2012;12:3127–31.
[7] Huang HS, Hainfeld JF. Intravenous magnetic nanoparticle cancer hyperthermia. Int J Nanomed 2013;8:2521–32.
[8] Balivada S, Rachakatla RS, Wang HW, Samarakoon TN, Dani RK, Pyle M, et al. A/C magnetic hyperthermia of melanoma mediated by iron(0)/iron oxide core/shell magnetic nanoparticles: a mouse study. BMC Cancer 2010;10:119.
[9] Hayashi K, Nakamura M, Sakamoto W, Yogo T, Miki H, Ozaki S, et al. Superparamagnetic nanoparticle clusters for cancer theranostics combining magnetic resonance imaging and hyperthermia treatment. Theranostics 2013;3:366–76.
[10] Yoo D, Lee JH, Shin TH. Theranostic magnetic nanoparticles Cheon. J Acc Chem Res 2011;44:863–74.
[11] Hilger I, Kaiser WA. Iron oxide-based nanostructures for MRI and magnetic hyperthermia. Nanomedicine 2012;7:1443–59.
[12] Mornet S, Vasseur S, Grasset F, Duguet E. Magnetic nanoparticle design for medical diagnosis and therapy. J Mater Chem 2004;14:2161–75.
[13] Jang JT, Nah H, Lee JH, Moon SH, Kim MJ, Cheon J. Critical enhancements of MRI contrast and hyperthermic effects by dopant-controlled magnetic nanoparticles. Angew Chem Int Ed 2009;48:1234–8.
[14] Xie J, Yan CZ, Zhang Y, Gu N. Shape evolution of "multibranched" Mn–Zn ferrite nanostructures with high performance: a transformation of nanocrystals into nanoclusters. Chem Mater 2013;25:3702–9.
[15] Bao NZ, Shen LM, Wang YHA, Ma JX, Mazumdr D, Gupta A. Controlled growth of monodisperse self-supported superparamagnetic nanostructures of spherical and rod-like $CoFe_2O_4$ nanocrystals. J Am Chem Soc 2009;131:12900–1.
[16] Bao NZ, Shen LM, An W, Padhan P, Turner CH, Gupta A. Formation mechanism and shape control of monodisperse magnetic $CoFe_2O_4$ nanocrystals. Chem Mater 2009;21:3458–68.
[17] Kumagai M, Sarma TK, Cabral H, Kaida S, Sekino M, Herlambang N. Enhanced in vivo magnetic resonance imaging of tumors by PEGylated iron-oxide–gold core–shell nanoparticles with prolonged blood circulation properties. Macromol Rapid Commun 2010;31:1521–8.
[18] Tong S, Hou SJ, Zheng ZL, Zhou J, Bao G. Coating optimization of superparamagnetic iron oxide nanoparticles for high T2 relaxivity. Nano Lett 2010;10:4607–13.
[19] Gu L, Fang RH, Sailor MJ, Park JH. In vivo clearance and toxicity of monodisperse iron oxide nanocrystals. ACS Nano 2012;6:4947–54.
[20] Ma Y, Tong S, Bao G, Gao C, Dai ZF. Indocyanine green loaded SPIO nanoparticles with phospholipid-PEG coating for dual-modal imaging and photothermal therapy. Biomaterials 2013;34:7706–14.
[21] May JP, Li SD. Hyperthermia-induced drug targeting. Expert Opin Drug Deliv 2013;10:511–27.
[22] Bae KH, Park M, Do MJ, Lee N, Ryu JH, Kim GW, et al. Chitosan oligosaccharide-stabilized ferrimagnetic iron oxide nanocubes for magnetically modulated cancer hyperthermia. ACS Nano 2012;6:5266–73.
[23] Chatterjee DK, Diagaradjane P, Krishnan S. Nanoparticle-mediated hyperthermia in cancer therapy. Ther Deliv 2011;2:1001–14.
[24] Stone R, Willi T, Rosen Y, Mefford OT, Alexis F. Targeted magnetic hyperthermia. Ther Deliv 2011;2:815–38.
[25] Ren YY, Zhang HJ, Chen BA, Cai XH, Liu R, Xia GH, et al. Multifunctional magnetic Fe_3O_4 nanoparticles combined with chemotherapy and hyperthermia to overcome multidrug resistance. J Nanomed 2012;7:2261–9.
[26] Jun YW, Huh YM, Choi JS, Lee JH, Song HT, Kim S, et al. Nanoscale size effect of magnetic nanocrystals and their utilization for cancer diagnosis via magnetic resonance imaging. J Am Chem Soc 2005;127:5732–3.
[27] Song MJ, Zhang Y, Hu SL, Song LN, Dong JL, Chen ZP, et al. Influence of morphology and surface exchange reaction on magnetic properties of monodisperse magnetite nanoparticles. Coll Surf A Physicochem Eng Asp 2012;408:114–21.
[28] Harvey AE, Smart JA, Amis ES. Simultaneous spectrophotometric determination of iron(II) and total iron with 1,10-phenanthroline. Anal Chem 1955;27:26–9.
[29] Maeng JH, Lee DH, Jung KH, Bae YH, Park IS, Jeong S, et al. Multifunctional doxorubicin loaded superparamagnetic iron oxide nanoparticles for

chemotherapy and magnetic resonance imaging in liver cancer. Biomaterials 2010;31:4995–5006.
[30] Chen WH, Xu XD, Jia HZ, Lei Q, Luo GF, Cheng SX, et al. Therapeutic nanomedicine based on dual-intelligent functionalized gold nanoparticles for cancer imaging and therapy in vivo. Biomaterials 2013;34:8798–807.
[31] Song LN, Zang FC, Song MJ, Chen G, Zhang Y, Gu N. Effective PEGylation of Fe_3O_4 nanomicelles for in vivo MR imaging. J Nanosci Nanotechnol 2014;14:1–8.
[32] Wang HS, Fei BW. Diffusion-weighted MRI for monitoring tumor response to photodynamic therapy. J Magn Reson Imaging 2010;32:409–17.
[33] Turkbey B, Aras O, Karabulut N, Turgut AT, Akpınar E, Alibek S, et al. Diffusion-weighted MRI for detecting and monitoring cancer: a review of current applications in body imaging. Diagn Interv Radiol 2012;18:46–59.
[34] Li ZM, Zhao YW, Zhao CJ, Zhang XP, Chen LJ, Wei YQ, et al. Hyperthermia increases the therapeutic efficacy of survivinT34A in mouse tumor models. Cancer Biol Ther 2011;12:523–30.
[35] Nishimura Y, Shibamoto Y, Jo S, Akuta K, Hiraoka M, Takahashi M, et al. Relationship between heat-induced vascular damage and thermosensitivity in four mouse tumors. Cancer Res 1988;48:7226–30.
[36] Roca C, Primo L, Valdembri D, Cividalli A, Declerck P, Carmeliet P, et al. Hyperthermia inhibits angiogenesis by a plasminogen activator inhibitor 1-dependent mechanism. Cancer Res 2003;63:1500–7.
[37] Davis ME, Chen Z, Shin DM. Nanoparticle therapeutics: an emerging treatment modality for cancer. Nat Rev Drug Discov 2008;7:71–82.
[38] Alexis F, Pridgen E, Molnar LK, Farokhzad OC. Factors affecting the clearance and biodistribution of polymeric nanoparticles. Mol Pharmacol 2008;5:505–15.
[39] Longmire M, Choyke PL, Kobayashi H. Clearance properties of nano-sized particles and molecules as imaging agents: considerations and caveats. Nanomedicine (Lond) 2008;3:703–17.
[40] Barreto JA, O'Malley W, Kubeil M, Graham B, Stephan H, Spiccia L. Nanomaterials: applications in cancer imaging and therapy. Adv Mater 2011;23:18–40.
[41] Branquinho LC, Carriao MS, Costa AS, Zufelato N, Sousa MH, Miotto R, et al. Effect of magnetic dipolar interactions on nanoparticle heating efficiency: implications for cancer hyperthermia. Sci Rep 2013;3:1–10.
[42] Stanley SA, Gagner JE, Damanpour S, Yoshida M, Dordick JS, Friedman JM. Radio-wave heating of iron oxide nanoparticles can regulate plasma glucose in mice. Science 2012;336:604–7.

Please cite this article in press as: Xie J, et al., High-performance PEGylated Mn–Zn ferrite nanocrystals as a passive-targeted agent for magnetically induced cancer theranostics, Biomaterials (2014), http://dx.doi.org/10.1016/j.biomaterials.2014.07.019